Carbohydrate Polymers 84 (2011) 329–334

Contents lists available at ScienceDirect

Carbohydrate Polymers

journal homepage: www.elsevier.com/locate/carbpol

Enhanced mechanical performance of poly(propylene carbonate) via hydrogen bonding interaction with *o*-lauroyl chitosan

Yusheng Qin [a], Lijie Chen [a,b], Xianhong Wang [a,*], Xiaojiang Zhao [a], Fosong Wang [a]

[a] Key Laboratory of Polymer Ecomaterials, Changchun Institute of Applied Chemistry, Chinese Academy of Sciences, Renmin Street 5625, Changchun 130022, PR China
[b] Graduate School of Chinese Academy of Sciences, Beijing 100039, PR China

ARTICLE INFO

Article history:
Received 25 September 2010
Accepted 18 November 2010
Available online 25 November 2010

Keywords:
Poly(propylene carbonate)
o-Lauroyl chitosan
Polymer blend
Hydrogen bonding

ABSTRACT

Biodegradable poly(propylene carbonate) (PPC) was blended with *o*-lauroyl chitosan (OCS) by solution casting using chloroform as common solvent. FTIR and XPS confirmed hydrogen bonding interaction between PPC and OCS, which was saturated when OCS loading reached 20 wt%. Because of the hydrogen bonding interaction, a 2–3 °C increase in glass transition temperature and a 5% improvement (46–53 °C) in weight loss temperature ($T_{5\%}$) were observed in the PPC/OCS blend with OCS loading of 10–20 wt%. The interaction was beneficial to improving the mechanical performance of PPC. The tensile strength, elongation at break, and Young's modulus of the pure PPC film were 31 MPa, 3.8%, and 392 MPa, respectively. For the blend with 10 wt% OCS loading, the effect of toughening was so substantial that the maximum elongation at break increased twofold to 8.1% and Young's modulus increased nearly threefold to 1014 MPa; the tensile strength and stress at break remained unchanged.

1. Introduction

Poly(propylene carbonate) (PPC) is an alternative copolymer of CO_2 and propylene oxide. It is a promising biodegradable polymer used in medical materials and food packaging because it utilizes CO_2 and shows good processability, providing transparent films with excellent oxygen barrier performance (Luinstra, 2008). However, PPC is amorphous with low glass transition temperature ($T_g \approx 35$ °C) due to the weak interchain interaction in this copolymer, limiting the use of plastics between 15 and 40 °C: it becomes brittle below 15 °C and quickly loses strength above 40 °C. Therefore, the poor mechanical performance of PPC requires improvement. For this purpose, chemical methods such as raising the molecular weight or regio-regularity of PPC, or introducing a third monomer by terpolymerization have been employed (Lu and Wang, 2004; Quan et al., 2003). Although the thermal and mechanical performance of PPC can be improved to a certain degree by chemical modification, physical blending remains attractive because it is simple and cost-effective. According to literature, PPC can be modified by blending with starch (Ma, Chang, Yu, & Wang, 2008), poly(lactic acid) (PLA) (Ma, Yu, & Wang, 2006), poly(3-hydroxybutyrate-co -3-hydroxyvalerate) (Peng et al., 2003a), poly(3-hydroxy butyrate) (Wang, Peng, & Dong, 2005), ethyl cellulose (Zhang et al., 2006), and octadecanoic acid (Yu et al., 2008). Nevertheless, even as the thermal stability of PPC is markedly enhanced, its brittleness remains a problem.

Chitosan is derived from abundant natural sources, such as various crustaceans, fungi, and lower plants. It is biodegradable and biocompatible because it consists of β-1,4-linked 2-acetamino-2-deoxy-D-glucopyranose and 2-amino-2-deoxy-D-gluco pyranose. Chitosan has received considerable attention in medical and pharmaceutical applications, including ophthalmology (Felt et al., 1999), implantations (Patashnik, Rabinovich, & Golomb, 1997), injections (Song et al., 2001), and so on. Because of its high T_g, however, it is difficult to melt process, similar to common thermal plastic materials; this property is attributed to its strong intramolecular hydrogen bonding and rigid structure (Brine, Sandford, & Zikakis, 1992), which may decompose before melting. In addition, chitosan is insoluble in most organic solvents, except in a few dilute aqueous acidic solutions.

The backbone of chitosan contains many amino and hydroxyl groups that may induce hydrogen bonding with carbonate units in PPC. This report aims to overcome the insolubility of chitosan in organic solvents by acylation using lauroyl chloride to produce a soluble chitosan derivative. The derivative was then used to prepare a polyblend with PPC. Hydrogen bonding interaction between PPC and *o*-lauroyl chitosan was investigated by Fourier transform infrared (FTIR) spectroscopy and X-ray photoelectron spectroscopy (XPS). The influence of hydrogen bonding interaction on the morphology, as well as the thermal and mechanical properties of PPC, is also disclosed.

* Corresponding author. Tel.: +86 431 85262250; fax: +86 431 85689095.
E-mail address: xhwang@ciac.jl.cn (X. Wang).

0144-8617/$ – see front matter © 2010 Elsevier Ltd. All rights reserved.
doi:10.1016/j.carbpol.2010.11.045

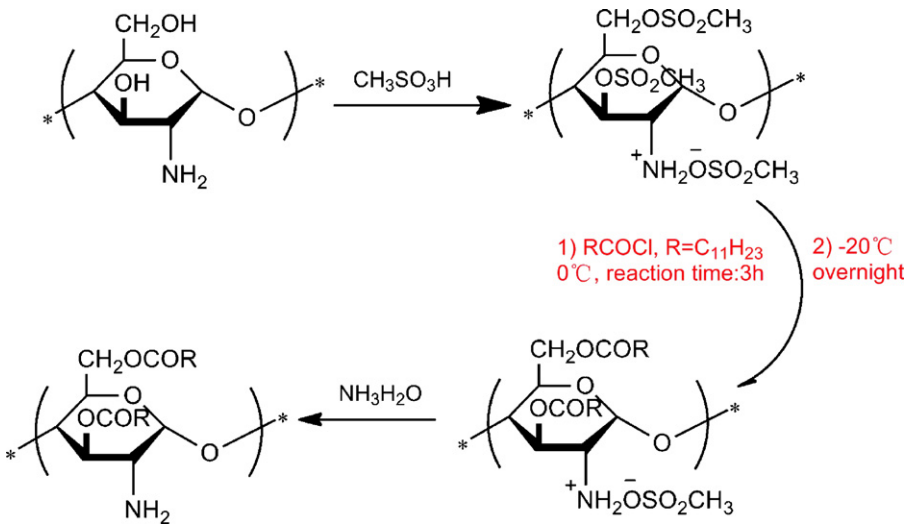

Scheme 1. Synthesis route for OCS.

2. Experimental

2.1. Materials

An 80-mesh chitosan powder with a 90.7% Ca deacetylation degree, was provided by the Jinan Haidebei Marine Bioengineering Co. (China). Lauroyl chloride, methanesulfonic acid (Sinopharm Chemical Reagent Co., China), and other reagents were used as received. PPC was supplied by the Inner Mongolia Mengxi High-tech Materials Co. (China) licensed under our laboratory. It was purified by a dissolution/precipitation procedure with acetone as solvent and ethanol as precipitate. The number average molecular weight (M_n) and polydispersity index (PDI) of the purified PPC were determined by GPC as 115 kg/mol and 2.89, respectively.

2.2. Synthesis and characterization of o-lauroyl chitosan (OCS)

The synthesis of OCS (Scheme 1) was performed in accordance with the Nishi method (Nishi, Ohnuma, Nishimura, Somorin, & Tokura, 1982). A calculated amount of chitosan powder was dissolved in methanesulfonic acid, with stirring. Lauroyl chloride was added to the solution and stirred at 0 °C for 3 h. The solution was then cooled to −20 °C and left to stand overnight. The suspension was neutralized with dilute aqueous ammonia to obtain a pH of 7.0. After filtration, the product was washed with methanol and dried at 50 °C under vacuum. The obtained OCS was characterized by FTIR spectroscopy, and its acylation degree was 1.8 as calculated from elemental analysis (EA).

FTIR (KBr): 3472, 3382, 2924, 2853, 1742, 1535, 1467, and 722 cm^{-1}.

EA data: found, C 67.84%; H 10.22%; N 1.96%; calculated for OCS with 1.8 degree of substitution, C 67.79%; H 10.32%; N 2.86%

2.3. Preparation of blend films

PPC and OCS of different weight ratios (100/0, 90/10, 80/20/, 70/30, 60/40) were dissolved in chloroform to prepare 1% (w/v) mixture solutions. After being stirred for 6 h, each solution was cast into a film and dried at 45 °C in vacuum for 48 h.

2.4. Characterization

FTIR spectra were obtained using a Bruker Tensor-27 spectrophotometer at 2 cm^{-1} resolution and 64 scans. The chloroform solutions of the samples were cast onto a KBr disk and dried at room temperature in vacuum for 24 h. EA was used to determine the substitution degree of the lauroyl groups on chitosan chains using an Elementar Vario EL.

XPS spectra were recorded on a Thermo ESCALAB 250 X-ray photoelectron spectroscope using Al Kα radiation (1486.6 eV) and a hemispherical energy analyzer using C1s peak of 284.6 eV as reference for binding energy (BE). All the spectra were curve fitted into a Gaussian function.

Differential scanning calorimetry (DSC) measurements were performed on a Perkin-Elmer DSC-7 instrument under a nitrogen atmosphere. For every test, the sample was heated from −50 to 150 °C in the first scan; the second heating scan was performed after cooling to −50 °C. T_g was recorded from the second heating curve to minimize the thermal history effect. Thermogravimetry analysis (TGA) was carried out on a Perkin-Elmer Pyris 1 TGA thermal analyzer from 40 to 500 °C under nitrogen protection at a heating rate of 10 °C/min.

Scanning electron microscopy (SEM) was conducted on an XL30 ESEM FEG (FEI Co.). The samples were broken after being cooled in liquid nitrogen, and the fracture surfaces were gold coated by ion sputtering for observation.

Mechanical performance analysis was carried out using a screw-driven universal testing machine (Z010, Zwick Co., Germany) equipped with a 10 KN electronic load cell and mechanical grips. The tests were conducted at 20 °C using a cross-head rate of 20 mm/min according to ASTM standards. Data were recorded as means of five parallel tests.

3. Results and discussion

3.1. Hydrogen-bonding interaction between PPC and OCS

The FTIR spectra of pure PPC and OCS, as well as those of the PPC/OCS blends with various compositions, are shown in Fig. 1. In the PPC spectra, the two strong absorption peaks observed at 1748 and 1233 cm^{-1} are attributed to the stretching vibrations of the C=O group and the C–O–C bond of the carbonate group, respectively (Liu, Zhao, Wang, & Wang, 2003). Compared with chitosan, the intensities of the amino and hydroxy absorption peaks at 3472 and 3382 cm^{-1} in pure OCS clearly decreased after acylation; the peaks were too weak to be observed in the FTIR spectra of the blend films because of low OCS content. Hence, we focused on the change in the absorption peaks of the C=O and C–O–C bonds in the polyblends.

Table 1
Curve fitting results of the C=O peaks and C–O–C bands in PPC/OCS blends.

PPC/OCS	C=O group in OCS		C=O group in PPC		O–C–O group in PPC	
	ν (cm^{-1})	$w_{1/2}$ (cm^{-1})	ν (cm^{-1})	$w_{1/2}$ (cm^{-1})	ν (cm^{-1})	$w_{1/2}$ (cm^{-1})
100/0	–	–	1747.8	33.2	1232.9	82.6
90/10	1740.3	18.0	1752.2	35.0	1236.2	88.4
80/20	1740.3	30.0	1754.0	42.5	1235.7	106.0
70/30	1741.5	27.3	1753.8	40.6	1234.7	97.8
60/40	1741.0	29.0	1752.8	40.0	1233.9	90.0
0/100	1741.9	34.8	–	–	–	–

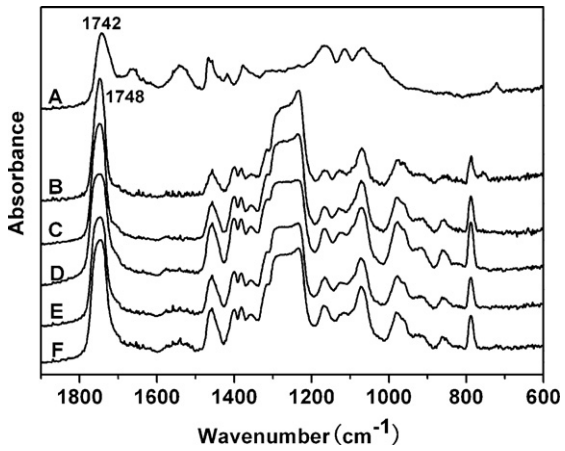

Fig. 1. FTIR spectra of OCS, PPC, and PPC/OCS blends at different compositions: (A) OCS; (B) PPC; (C) PPC/OCS = 90/10; (D) PPC/OCS = 80/20; (E) PPC/OCS = 70/30; and (F) PPC/OCS = 60/40.

All the spectra were normalized for convenient analysis. The characteristic peaks at around 1233 cm^{-1} in the blends were single and wholly attributed to the C–O–C groups in PPC because no absorption in this region was observed from the OCS spectra. Fig. 1 shows that when OCS loading in the blend increased to 20 wt%, the C–O–C absorption peak considerably broadened from 82.6 to 106 cm^{-1} with a blue shift at ca. 3 cm^{-1}. Although an overlap was observed in the strong absorption peak around 1750 cm^{-1}, ascribed to the stretching vibration of the C=O groups in PPC and OCS, the overlap can be separated into two bands by curve fitting analysis to more clearly observe the change in the C=O bands in PPC. As listed in Table 1, the peak at ca. 1741 cm^{-1} is assigned to the stretching vibration of the C=O group in OCS because the location of this peak was nearly unchanged at various OCS loadings. The half-height width ($w_{1/2}$) of the peak gradually diminished with decreasing OCS loading. The other peak is assigned to the C=O group in PPC. When OCS loading increased to 20 wt%, the peak moved from ca. 1748 cm^{-1} to 1754 cm^{-1}, and broadened with $w_{1/2}$ increasing from ca. 33 cm^{-1} to ca. 43 cm^{-1}, indicating that the carbonate groups of PPC can participate in intermolecular interaction with the NH and OH groups of OCS through hydrogen bonding – a behavior similar to the results in the PLA/chitosan blend system (Chen et al., 2005). When OCS content exceeded 20 wt%, the change in C=O absorption in PPC was negligible. Therefore, OCS content higher than 20 wt% may attain saturated interaction between PPC and OCS. Previous studies on the shifting and broadening variety of the corresponding absorption peaks can be regarded as a measure of intermolecular interaction (Coleman, Lichkus, & Painter, 1989).

Hydrogen bonding interaction is derived from the electron transfer between proton acceptors and proton donors; for NH and C=O groups, the electron density in N–H bonds may decrease, whereas that in the electron-withdrawing C=O group may increase. The BE of nitrogen in the XPS spectra (N_{1s}) can change, or a new peak with a higher band may appear (Chen et al., 2005). Fig. 2 shows the XPS spectra of N_{1s} in the blends, as well as in OCS. The BE values of the N_{1s} peak for the blends are summarized in Table 2. A single N_{1s} peak in OCS with a BE value of 399.6 eV was found (Chen et al., 2005). The N_{1s} peaks in the blends can be resolved into two contributions: one remained at 399.6 eV and a new peak appeared in the 400–400.4 eV range. Goh and Lee reported that a shift of about 1 eV for the N_{1s} peak in XPS spectra indicates hydrogen-bonding interaction, whereas a shift of about 2–2.5 eV was due to ionic interaction (Goh, Liu, Lee, & Huan, 1999). The high BE peaks at around 400 eV in the blends should be attributed to the hydrogen-bonded N–H bond. The fraction of the amino groups in OCS involved in hydrogen bonding interactions can be estimated from the area fraction of high BE peaks (Goh et al., 1999). When OCS increased from 10 to 20 wt%, the fraction of high BE peaks increased from 25.8% to 27.4%. Under higher OCS loading, the corresponding fraction of high BE peaks was kept constant at 20%, suggesting saturation of the hydrogen bonding interaction, a behavior in good agreement with the FTIR spectroscopy results. Therefore, the hydrogen bonding interaction between PPC and OCS was further confirmed by the XPS analysis.

3.2. Thermal properties of the blend films

The TGA and DSC curves of the PPC/OCS blend films with various OCS contents are shown in Fig. 3. The main thermal properties for PPC, OCS, and the polyblends are summarized in Table 3.

According to the TGA curves, pure OCS exhibited thermal degradation in two stages: the 5% weight-loss temperature ($T_{5\%}$) and temperature at maximum degradation rates (T_{max}, 180 and 267 °C, respectively); both were lower than those for chitosan (Wan, Wu, Yu, & Wen, 2006). This result is probably due to the existence of lauroyl groups in OCS, impairing intramolecular hydrogen bonding. However, the $T_{5\%}$ of the PPC/OCS blend films with 10 and 20 wt% OCS loading increased to 265 and 258 °C, respectively, both of which are much higher than that of pure PPC (212 °C). A further increase in OCS content did not lead to a considerable increase in $T_{5\%}$. All the blends showed remarkably higher T_{max} than did pure OCS or PPC, indicating that the thermal stability of PPC substantially improved. This improvement in stability is attributed to the exis-

Table 2
XPS analysis of PPC/OCS blends and pure OCS.

PPC/OCS (w/w)	0/100	90/10	80/20	70/30	60/40
N_{1s} BE peak (eV)	399.6	399.6	399.6	399.6	399.6
		400.0	400.1	400.3	400.4
Position of N_{1s} high-BE peaks (eV)		400.0	400.1	400.3	400.4
Fraction of N_{1s} high-BE peak (%)		25.8	27.4	20.2	20.3

Table 3
Thermal properties for PPC, OCS, and their blends.

OCS ratio (wt%)	0	10	20	30	40	100
$T_{5\%}$ (°C)	212.2	265.0	257.6	229.6	218.5	179.7
T_{max} (°C)	226.4	294.6	295.8	301.1	302.0	267.3
T_g (°C)	34.10	37.35	36.15	36.97	35.51	–

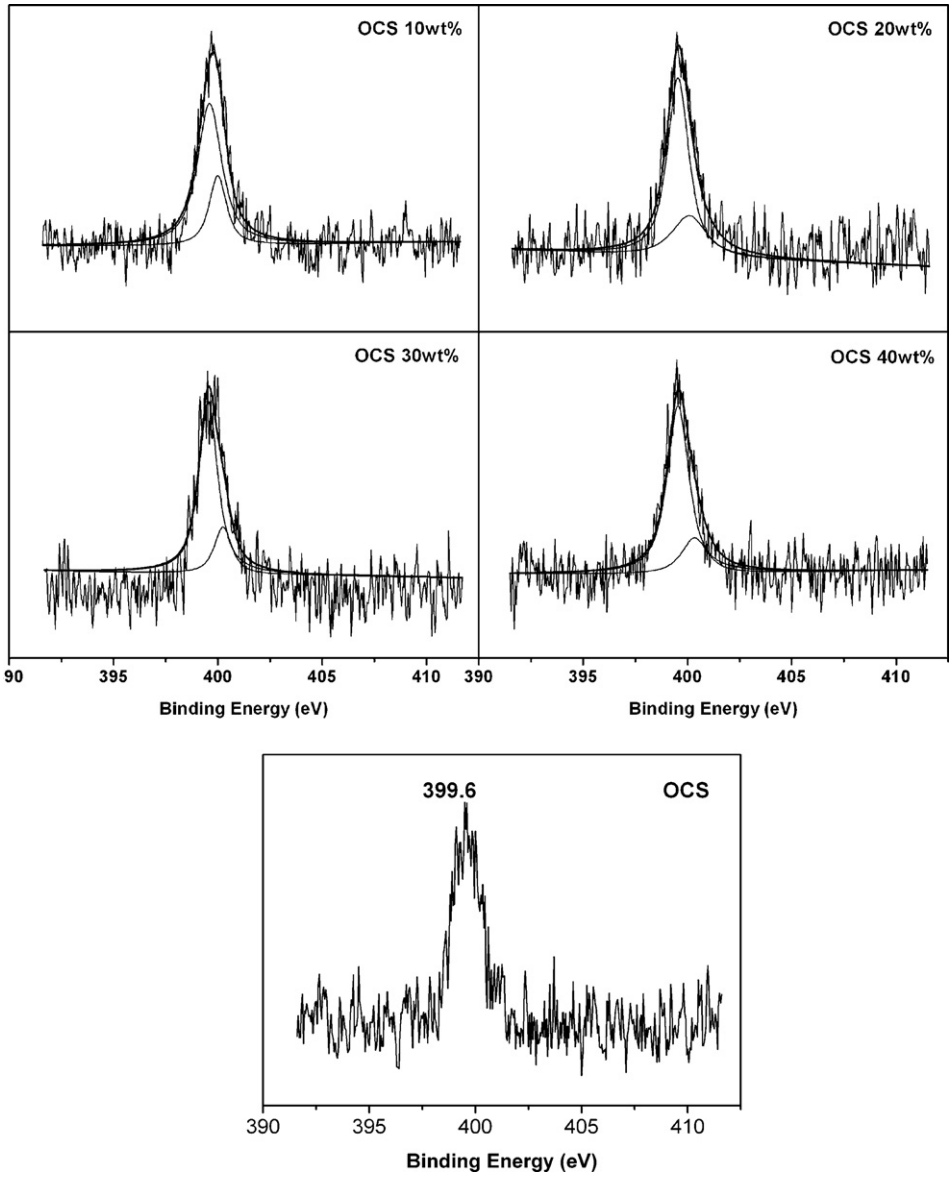

Fig. 2. N1s spectra of OCS and PPC/OCS blends at different compositions.

tence of effective hydrogen bonding interactions between PPC and OCS, which weakened the random main chain thermal scission, as well as chain unzipping reaction, of PPC (Peng et al., 2003b).

Although T_g is an important parameter for assessing the miscibility of two polymers, no obvious T_g or any other endothermic peak was observed in pure OCS in the second heating run. This finding is mainly associated with the semicrystallinity, rigid structure, and strong intramolecular hydrogen bond of pure OCS, hindering the formation of a mobile, amorphous phase at T_g (Peesan, Supaphol, & Rujiravanit, 2005). The T_g of the blends with 10 or 20 wt% OCS were 37.35 and 36.15 °C, respectively (higher than 34 °C of pure PPC). The increase in T_g must also result from the hydrogen bonding interaction between PPC and OCS, which restricted the mobility of the PPC chain segment.

3.3. Phase morphology

The phase morphology of the PPC/OCS blend was analyzed by XRD and SEM. Fig. 4 shows that phase separation occurred in the PPC/OCS blends and spherites appearing as a dispersion phase in the continuous matrix. In PPC-rich compositions, the continuous matrix should be composed of PPC, whereas dispersive spherites are formed by OCS. Fig. 4A–C was observed under 6400 magnification using a scanning electron microscope; the magnification for the blend with 40 wt% OCS loading was diminished to 3200 to better evaluate the size of the dispersive phase and distribution of the spherite diameter because the dimension of the OCS particle was too large under 6400 magnification. The spherite of about 1 μm was embedded into the PPC matrix and the interface between the two phases was obscure, suggesting good interfacial adhesion. With 20 wt% OCS loading, both the diameter and number of spherites gradually increased; however, the distribution of spherite diameter was still narrow (Fig. 4B). The phase morphology of the blend with 30 wt% OCS content exhibited apparent discrepancy, as seen in Fig. 4C; the diameter of the dispersive phase differed between 1 and 5 μm, and the spherites piled up in a disorderly manner and even debonded with the PPC matrix. A visible space between the spheres and the matrix was observed, which may be the reason why the hydrogen bonding interaction between PPC and OCS reached saturation at 20 wt% OCS loading. When the OCS content in the

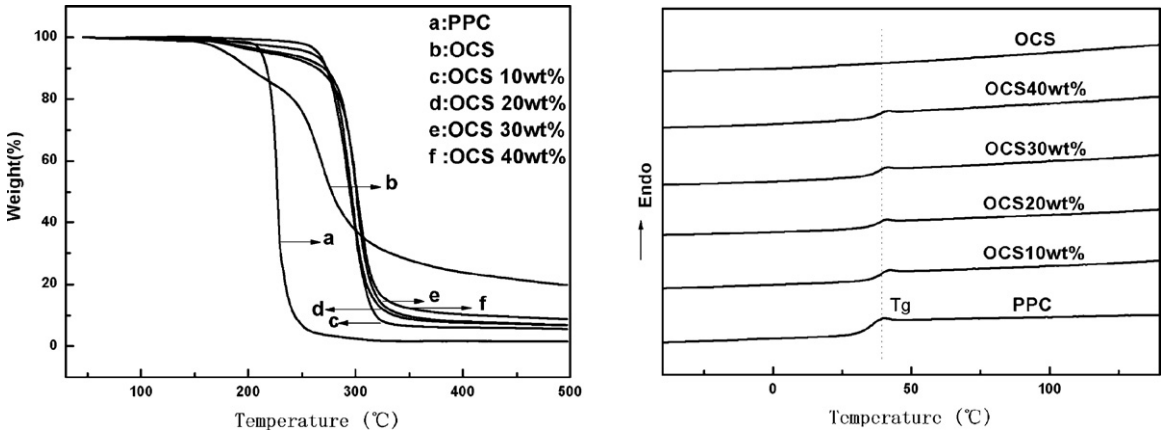

Fig. 3. TGA and DSC curves of PPC/OCS blends at various OCS loadings.

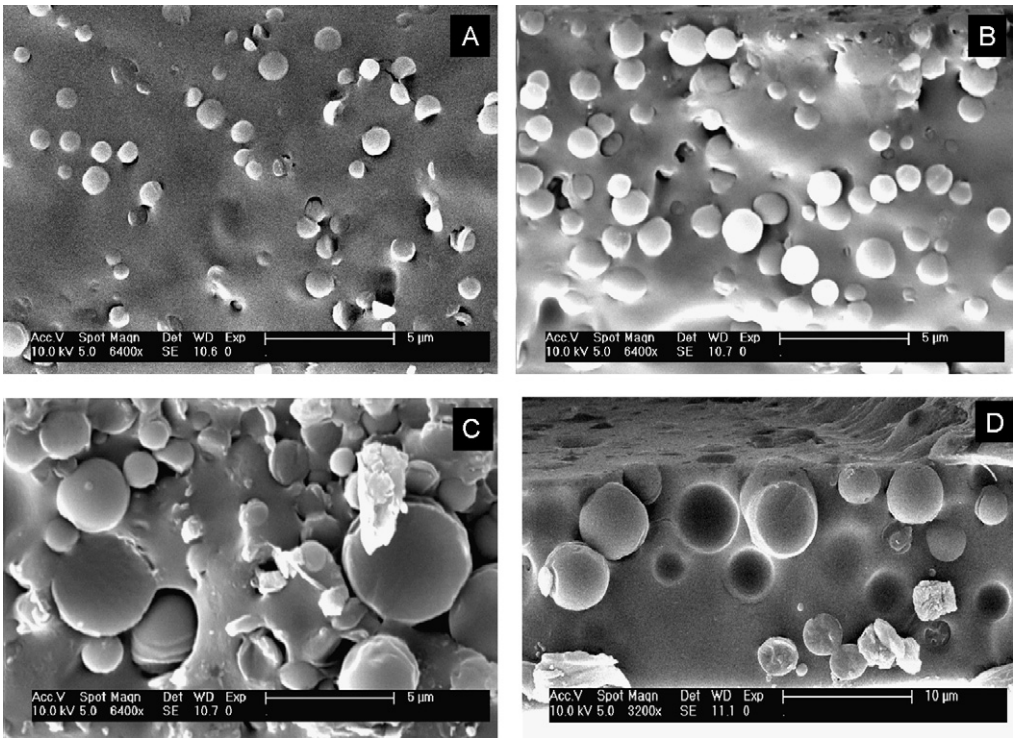

Fig. 4. SEM images of blends with different OCS loadings: (A) 10 wt% OCS, (B) 20 wt% OCS, (C) 30 wt% OCS, and (D) 40 wt% OCS.

polyblend increased to 40 wt%, the number of spherites decreased, and the size of the particles increased varying from 3 to 5 μm.

3.4. Mechanical properties

The effect of OCS content on the mechanical properties of the blend films is shown in Table 4. The tensile strength, elongation at break, and Young's modulus of the pure PPC film were 31 MPa, 3.8%, and 392 MPa, respectively. For the blend with 10 wt% OCS loading, toughening was observed, and the maximum elongation at break increased twofold to 8.1%, Young's modulus increased nearly threefold to 1014 MPa, and the tensile strength and stress at break remained unchanged. The improvement in mechanical properties is associated with hydrogen bonding interaction between two polymers, as well as the effective size and distribution of the dispersive phase (Mezzenga, Boogh, & Manson, 2001; Mezzenga, Boogh, Pettersson, & Manson, 2000). This improvement occurs because hydrogen bonding can enhance the interfacial adhesion of polymer composition, and therefore improves mechanical properties, making the material especially favorable for enhancing tensile strength. When OCS loading was above 20 wt%, Young's modulus, stress, and elongation at break showed a tendency to decrease probably because of serious phase separation. The effective particle size for PPC toughening may be 1–2 μm.

Table 4
Mechanical properties of pure PPC and PPC/OCS blends.

OCS ratio (wt%)	Young's modulus (MPa)	Stress at break (MPa)	Tensile strength (MPa)	Elongation at break (%)
0	392	21	31	3.8
10	1014	21	32	8.1
20	1403	17	29	6.2
30	1118	20	24	3.7
40	850	17	19	3.0

4. Conclusions

Soluble *o*-lauroyl chitosan was synthesized by acylation of chitosan, and PPC/OCS blend films were prepared by casting chloroform solutions. FTIR spectroscopy and XPS results indicate intermolecular hydrogen bonding between the two components, and the interaction reached saturation at 20 wt% OCS loading. Such effects are mainly induced by serious phase separation as confirmed by the SEM images. The addition of OCS markedly improved the thermal stability of PPC, and the T_g of PPC increased by 2–3 °C when 10–20 wt% OCS was added. Because of the hydrogen bonding, efficient particle diameters for dispersed phase toughening, and narrow size distribution, both the elongation at break and Young's modulus of the blend films with OCS loading of 10–20 wt% were considerably enhanced. The tensile strength and stress at break slightly decreased compared with the corresponding data of pure PPC.

Acknowledgment

This work was financially supported by the National Natural Science Foundation of China (Grant nos. 20634040 and 50903084).

References

Brine, C. J., Sandford, P. A., & Zikakis, J. P. (1992). *Advances in chitin and chitosan*. New York: Elsevier Applied Science.

Chen, C., Dong, L., & Cheung, M. K. (2005). Preparation and characterization of biodegradable poly(L-lactide)/chitosan blends. *European Polymer Journal*, *41*(5), 958–966.

Chen, C., Zhou, X. S., Zhuang, Y. G., & Dong, L. S. (2005). Thermal behavior and intermolecular interactions in blends of poly(3-hydroxybutyrate) and maleated poly(3-hydroxybutyrate) with chitosan. *Journal of Polymer Science Part B: Polymer Physics*, *43*(1), 35–47.

Coleman, M. M., Lichkus, A. M., & Painter, P. C. (1989). Thermodynamics of hydrogen-bonding in polymer blends. 3. Experimental studies of blends involving poly(4-vinylphenol). *Macromolecules*, *22*(2), 586–595.

Felt, O., Furrer, P., Mayer, J. M., Plazonnet, B., Buri, P., & Gurny, R. (1999). Topical use of chitosan in ophthalmology: Tolerance assessment and evaluation of precorneal retention. *International Journal of Pharmaceutics*, *180*(2), 185–193.

Goh, S. H., Liu, Y., Lee, S. Y., & Huan, C. H. A. (1999). Miscibility and interactions in blends and complexes of poly(N-acryloyl-N′-phenylpiperazine) with acidic polymers. *Macromolecules*, *32*(25), 8595–8602.

Liu, B. Y., Zhao, X. J., Wang, X. H., & Wang, F. S. (2003). Copolymerization of carbon dioxide and propylene oxide with neodymium trichloroacetate-based coordination catalyst. *Polymer*, *44*(6), 1803–1808.

Lu, X. B., & Wang, Y. (2004). Highly active, binary catalyst systems for the alternating copolymerization of CO_2 and epoxides under mild conditions. *Angewandte Chemie International Edition*, *43*(27), 3574–3577.

Luinstra, G. A. (2008). Poly(propylene carbonate), old copolymers of propylene oxide and carbon dioxide with new interests: Catalysis and material properties. *Polymer Reviews*, *48*(1), 192–219.

Ma, X. F., Chang, P. R., Yu, J. G., & Wang, N. (2008). Preparation and properties of biodegradable poly(propylene carbonate)/thermoplastic dried starch composites. *Carbohydrate Polymers*, *71*(2), 229–234.

Ma, X. F., Yu, J. G., & Wang, N. (2006). Compatibility characterization of poly(lactic acid)/poly(propylene carbonate) blends. *Journal of Polymer Science Part B: Polymer Physics*, *44*(1), 94–101.

Mezzenga, R., Boogh, L., & Manson, J. A. E. (2001). A review of dendritic hyperbranched polymer as modifiers in epoxy composites. *Composites Science and Technology*, *61*(5), 787–795.

Mezzenga, R., Boogh, L., Pettersson, B., & Manson, J. A. E. (2000). Chemically induced phase separated morphologies in epoxy resin-hyperbranched polymer blends. *Macromolecular Symposia*, *149*, 17–22.

Nishi, N., Ohnuma, H., Nishimura, S., Somorin, O., & Tokura, S. (1982). Studies on chitin. 7. Preparations of para-substituted benzoylchitins. *Polymer Journal*, *14*(11), 919–923.

Patashnik, S., Rabinovich, L., & Golomb, G. (1997). Preparation and evaluation of chitosan microspheres containing bisphosphonates. *Journal of Drug Targeting*, *4*(6), 371–380.

Peesan, M., Supaphol, P., & Rujiravanit, R. (2005). Preparation and characterization of hexanoyl chitosan/polylactide blend films. *Carbohydrate Polymers*, *60*(3), 343–350.

Peng, S. W., An, Y. X., Chen, C., Fei, B., Zhuang, Y. G., & Dong, L. S. (2003a). Miscibility and crystallization behavior of poly(3-hydroxyvalerate-co-3-hydroxyvalerate)/poly(propylene carbonate) blends. *Journal of Applied Polymer Science*, *90*(14), 4054–4060.

Peng, S. W., An, Y. X., Chen, C., Fei, B., Zhuang, Y. G., & Dong, L. S. (2003b). Thermal degradation kinetics of uncapped and end-capped poly(propylene carbonate). *Polymer Degradation and Stability*, *80*(1), 141–147.

Quan, Z. L., Min, J. D., Zhou, Q. H., Xie, D., Liu, J. J., Wang, X. H., et al. (2003). Synthesis and properties of carbon dioxide–epoxides copolymers from rare earth metal catalyst. *Macromolecular Symposia*, *195*, 281–286.

Song, J. S., Suh, C. H., Park, Y. B., Lee, S. H., Yoo, N. C., Lee, J. D., et al. (2001). A phase I/Iia study on intra-articular injection of holmium-166-chitosan complex for the treatment of knee synovitis of rheumatoid arthritis. *European Journal of Nuclear Medicine*, *28*(4), 489–497.

Wan, Y., Wu, H., Yu, A. X., & Wen, D. J. (2006). Biodegradable polylactide/chitosan blend membranes. *Biomacromolecules*, *7*(4), 1362–1372.

Wang, X. Y., Peng, S. W., & Dong, L. S. (2005). Effect of poly(vinyl acetate) (Pvac) on thermal behavior and mechanical properties of poly(3-hydroxybutyrate)/poly(propylene carbonate) (Phb/Ppc) blends. *Colloid and Polymer Science*, *284*(2), 167–174.

Yu, T., Zhou, Y., Zhao, Y., Liu, K. P., Chen, E. Q., Wang, D. J., et al. (2008). Hydrogen-bonded thermostable liquid crystalline complex formed by biodegradable polymer and amphiphilic molecules. *Macromolecules*, *41*(9), 3175–3180.

Zhang, Z. H., Zhang, H. L., Zhang, Q. X., Zhou, Q. H., Zhang, H. F., Mo, Z. S., et al. (2006). Thermotropic liquid crystallinity, thermal decomposition behavior, and aggregated structure of poly(propylene carbonate)/ethyl cellulose blends. *Journal of Applied Polymer Science*, *100*(1), 584–592.